UNIVERSITY
OF TRENTO

**DIPARTIMENTO DI INGEGNERIA E SCIENZA DELL'INFORMAZIONE**

38123 Povo – Trento (Italy), Via Sommarive 14
http://www.disi.unitn.it

# MULTICRACK DETECTION IN TWO-DIMENSIONAL STRUCTURES BY MEANS OF GA-BASED STRATEGIES

M. Benedetti, M. Donelli, and A. Massa

January 2007

Technical Report # DISI-11-073

# Multicrack Detection in Two-Dimensional Structures by means of GA-based Strategies

M. Benedetti, M. Donelli, *Member, IEEE*, and A. Massa, *Member, IEEE*,

Department of Information and Communication Technology

University of Trento, Via Sommarive 14, 38050 Trento - Italy

Tel. +39 0461 882057, Fax +39 0461 882093

E-mail: *andrea.massa@ing.unitn.it,*

{*manuel.benedetti, massimo.donelli*} *@dit.unitn.it*

Web-site: *http://www.eledia.ing.unitn.it*

# Multicrack Detection in Two-Dimensional Structures by means of GA-based Strategies

M. Benedetti, M. Donelli, and A. Massa

**Abstract**

This paper proposes a methodological approach for the detection of multiple defects inside dielectric or conductive media. Two innovative algorithms are developed starting from the inverse scattering equations solved by means of different optimization strategies. In the first implementation, a hierarchical strategy based on parallel-subprocesses is considered, whereas the second algorithm employs a single-process architecture. Whatever the implementation, the arising cost function is minimized through a suitable hybrid-coded genetic algorithm, whose individuals encode the problem unknowns. In order to achieve a computational saving, the formulation based on the inhomogeneous Green's function is adopted and each crack-region is parametrized by means of a selected set of descriptive parameters. The approach as well as its different implementations are assessed through a selected set of numerical experiments and in comparison with previously developed single-crack inverse scattering methods.

***Key-words***: Non-destructive Testing and Evaluation, Microwave Imaging, Multicrack Detection

# 1 Introduction

Nondestructive Evaluation and Testing (NDE/NDT) is an interdisciplinary research area devoted to the development of advanced sensors, measurement technologies, and imaging techniques for the characterization of materials and structures in a non-destructive fashion. Non-destructive evaluation (NDE) and testing (NDT) are mandatory in many industrial processes that require an accurate analysis of dielectric or conductive structures (e.g., industrial products and artefacts).

As far as the state-of-the-art is concerned, ultrasonics [1], $\chi$ and $\gamma$-rays [2][3], infrared [4] and eddy currents [5], are the methodologies mainly used in dealing with NDE/NDT problems. Recently, some "emerging" technologies such as microwaves are appearing in "Subsurface Sensing" methods for the nondestructive evaluation (see [6][7][8][9][10] and the references therein for a general overview) and now, in some applications, the employment of interrogating microwaves is recognized as a suitable diagnostic tool [11]-[13]. The main reasons of the growing interest and rapid development of microwave-based methodologies can be summarized by the following key-points: ($a$) electromagnetic fields in the microwaves range penetrate all materials (unless ideal conductors) and the scattered fields are representative of the overall volume of the object under test and not only of its surface; ($b$) microwave imaging modalities are very sensitive to the water content of the specimen; ($c$) microwave sensors can be used without mechanical contacts with the specimen, as well. Moreover, microwave technologies can be considered complementary approaches to conventional inspection techniques guaranteeing non-invasive measurements and avoiding collateral effects on the specimen under test (being safe non-ionizing radiations).

In the framework of microwave methodologies, a further advance is represented by imaging techniques based on inverse scattering approaches [14]-[18], where a complete image of the structure under test is looked for. Unfortunately, these techniques are characterized by several drawbacks such as ill-position and non-linearity as well as the presence of local minima that partially prevent their use in industrial applications (unlike "passive" techniques) [11]. Therefore, in order to allow an effective technological transfer in the framework of industrial processes, other developments are mandatory. Let us consider the area of post-processing techniques for the diagnosis of the specimen under test starting

from the analysis of sensed data. Currently, the real-time monitoring is strongly limited by the low-speed of the reconstruction methods. Moreover, the wavelength of the probing electromagnetic source strongly limits the achievable spatial resolution or it requires high computational costs for obtaining a detailed reconstruction.

However, in the framework of inverse scattering techniques, dealing with the detection of defects (also indicated as "cracks" in the following) in known host structures seems to be closer to a realistic application because of the large amount of available *a-priori* information on the problem in hand. Such a topic has been effectively addressed in [19], [20], and [21]. However, the proposed approaches demonstrated their feasibility and effectiveness in simplified geometric configurations characterized by the presence of a single defect.

In order to consider more complex and realistic scenarios (e.g., multiple defects, irregular shapes of the defects, etc...), this work presents two innovative NDE/NDT strategies aimed at detecting the presence of more than one defective region inside a dielectric or conductive host-medium. Since there is the *a-priori* knowledge of the unperturbed geometry, the cracks are defined as inclusions in a known structure and approximated with a limited set of essential parameters. Such a parameterization and the use of a suitable Green's function allow a reduction of the number of unknowns and consequently a non-negligible computational saving during the reconstruction process carried out in terms of the optimization of a suitable cost function.

As far as the proposed implementations are concerned, the main difference lies in the architecture of the solution procedure and, consequently, in customized and innovative optimizations based on a Genetic Algorithm (GA). The former strategy is based on a hierarchical implementation, which considers a set of parallel sub-processes, each one inspecting on a solution with a different fixed number of cracks. The latter deals with a single optimization process aimed at looking for the best reconstruction among different crack-length solutions.

The paper is structured as follows. Section 2 provides the mathematical formulation for the inverse scattering approach to the reconstruction of multiple-defects in a two-dimensional scenario. In Section 3, the two implementations of the method are presented

focusing on the optimization processes. The capabilities and current limitations of the two strategies in dealing with NDE/NDT problems are analyzed in Section 4. Finally, in Section 5, a discussion follows and possible future developments are sketched.

## 2 Mathematical Formulation

Let us consider a cylindric geometry where an area under test $H$ is occupied by a known host medium characterized by an object function $\tau_H(x,y) = \varepsilon_H - 1 - j\frac{\sigma_H}{2\pi f \varepsilon_0}$, $\varepsilon_H$ and $\sigma_H$ being its dielectric permittivity and conductivity, respectively ($f$ is the working frequency). As shown in Fig. 1, such a region lies in a homogeneous background whose electromagnetic properties, without loss of generality, are that of the vacuum $(\varepsilon_0, \sigma_0)$. A set of $C$ defects $D_i$, $i = 1, ..., C$, belongs to $H$. The geometric and electromagnetic characteristics of the regions $D_i$ are unknown as well as their number. The two-dimensional scenario is probed by $V$ electromagnetic TM plane waves with electric incident fields linearly-polarized along the axis of symmetry of the structure under test, $\underline{E}^v_{inc}(\underline{r}) = E^v_{inc}(x,y)\,\underline{\hat{z}}$, $v = 1, ..., V$. According to the inverse scattering equations [22], the electric field induced in the "*investigation domain*" $H$ is equivalent to that radiated in the free-space by an equivalent current density $J^v(x,y)$

$$E^v_{tot}(x,y) = E^v_{inc}(x,y) + \int\int_H J^v(x',y') G_0(x,y/x',y')\,dx'dy' \tag{1}$$

where $G_0$ is the free-space Green's function [19] and $J^v(x,y) = \tau(x,y)\,E^v_{tot}(x,y)$ being $\tau(x,y) = \varepsilon(x,y) - 1 - j\frac{\sigma(x,y)}{2\pi f \varepsilon_0}$. Equation (1) can be reformulated in terms of a differential equivalent current density $J^v_{D_i}(x,y)$ defined in $D_i$, $i = 1, ..., C$ and radiating in an inhomogeneous medium [23]. Accordingly, the electric field can be expressed as

$$\begin{aligned} E^v_{tot}(x,y) = E^v_{inc}(x,y) + \textstyle\int\int_H \tau_H(x',y')\,E^v_{tot\,(cf)}(x',y')\,G_0(x,y/x',y')\,dx'dy' + \\ + \textstyle\sum_{i=1}^{C} \int\int_{D_i} \tau_{D_i}(x',y')\,E^v_{tot\,(c),i}(x',y')\,G_1(x,y/x',y')\,dx'dy' \end{aligned} \tag{2}$$

where the second term on the right side of (2) is the electric field scattered from the host medium without the defect, $E^v_{tot\,(cf)}(x,y)$ being the electric field induced in the unper-

turbed domain $H$. The last term of (2) is concerned with the field distribution radiated by $J^v_{D_i}(x,y) = \tau_{D_i}(x,y)\, E^v_{tot\,(c),i}(x,y)$ where $\tau_{D_i}(x,y) = \tau(x,y) - \tau_H(x,y)$, $(x,y) \in D_i$, $i = 1, ..., C$ [20] are the differential object functions, $G_1$ being the inhomogeneous Green's function. By assuming the knowledge of the host medium (generally available), it is useful to rewrite (2) as follows:

$$E^v_{tot}(x,y) = E^v_{inc\,(cf)}(x,y) + \sum_{i=1}^{C} \int\int_{D_i} \tau_{D_i}(x',y')\, E^v_{tot\,(c),i}(x',y')\, G_1(x,y/x',y')\, dx'dy' \quad (3)$$

where $E^v_{inc\,(cf)}(x,y)$ is the electric field in the scenario under test without the defect, which can be computed off-line once.

In order to numerically deal with the scattering equations, let us discretize $H$ in $N$ square sub-domains [24]. Therefore, $D_i$ turns out to be filled by $P_i$ square pixels according to the crack size and the discretized operator $G_1$ can be easily computed [20] and stored in a $N \times N$ matrix, $[G_1]$. Thus, (3) becomes

$$[E^v_{tot}] = \left[E^v_{inc\,(cf)}\right] + \sum_{i=1}^{C} [G_{1,i}]\, [\tau_{D_i}]\, \left[E^v_{tot,i}\right] \quad (4)$$

where:

- $[E^v_{tot}]$ is a $N \times 1$ array whose $n$-th element is $E^v_{tot}(x_n, y_n)$, $(x_n, y_n) \in H$;
- $\left[E^v_{inc\,(cf)}\right] \triangleq [E^v_{inc}] + [G_o]\, [\tau_H]\, \left[E^v_{tot\,(cf)}\right]$ is a $N \times 1$ array whose $n$-th entry is the electric field without the defect at the $n$-th subdomain of $H$ given by $E^v_{inc\,(cf)}(x_n, y_n) = E^v_{inc}(x_n, y_n) + \int\int_H \tau_H(x',y')\, E^v_{tot\,(cf)}(x',y')\, G_0(x_n, y_n/x', y')\, dx'dy'$;
- $\left[E^v_{tot,i}\right]$ is a $P_i \times 1$ vector whose $p_i$-th entry identifies the value of the electric field in the $p_i$-th pixel of $D_i$, $i = 1, ..., C$;
- $[\tau_{D_i}]$ is a $P_i \times P_i$ diagonal matrix, whose non-null elements are the values of object function $\tau_{D_i}$ in the $P_i$ pixels of $D_i$;
- $[G_{1,i}]$ is the $i$-th inhomogeneous space Green's matrix of $N \times P_i$ elements derived from $[G_1]$ by selecting the rows related to the positions $p_i$ ($p_i = 1, ..., P_i$) of the pixels of $D_i$ in $H$.

Since the inhomogeneous operator $[G_{1,i}]$ determines the effects of the $i$-th differential equivalent current density located in the unknown region $D_i$, the scattering problem can be reformulated as the reconstruction of the differential object function $\tau_{D_i}$ in the set of pixels $p_i = 1, ..., P_i$ of $H$ where the defect is located. Moreover, in order to further decrease the number of unknowns by adding some *a-priori* assumptions, each region $D_i$ is approximated by a rectangular homogeneous domain properly parametrized. In particular, let us describe the $i$-th defect with the coordinates of the center of $D_i$,$(x_i, y_i)$, the length $L_i$, its side $W_i$, and the orientation $\theta_i$. Then, the $P_i$ diagonal entries of $[\tau_{D_i}]$ turn out to be

$$\tau_{D_i}\rfloor_{n,n} = \begin{cases} \tau(x_n, y_n) - \tau_H(x_n, y_n) & \text{if } \xi \in \left[-\frac{L_i}{2}, \frac{L_i}{2}\right] \text{ and } \zeta \in \left[-\frac{W_i}{2}, \frac{W_i}{2}\right] \\ 0 & \text{otherwise} \end{cases} \tag{5}$$

where $\xi = (x_n - x_i)\cos\theta_i + (y_n - y_i)\sin\theta_i$, $\zeta = (x_n - x_i)\sin\theta_i + (y_n - y_i)\cos\theta_i$, and $n = 1, \ldots, P_i$.

Moreover, since the electric field induced in $D_i$ is unknown as well, the set of parameters to be retrieved during the reconstruction is

$$\chi = \left\{C;\, \Upsilon_i,\, i = 1, ..., C;\, \left[E^v_{tot,i}\right],\, i = 1, ..., C\right\} \tag{6}$$

where $\Upsilon_i = [(x_i, y_i)\,; L_i; W_i; \theta_i]$ and $\left[E^v_{tot,i}\right] = \{E^v_{tot}\,(x_{p_i}, y_{p_i})\,,\, p_i = 1, \ldots,\, P_i\}$, $i = 1, \ldots,\, C$. In order to determine the optimal solution $\chi_{opt}$ of the reconstruction problem from the knowledge of the field measured in an external observation domain $O$ [i.e., $E^v_{tot}(x_m, y_m)$, $m = 1, ..., M$, $(x_m, y_m) \in O \notin H$], of the field at the same locations but without the defect, $E^v_{tot\,(cf)}(x_m, y_m)$, and of the field without the defect in the investigation domain $H$ [i.e., $E^v_{inc}(x_n, y_n)$, $n = 1, ..., N$, $(x_n, y_n) \in H$], the problem in hand is recast as an optimization one through the definition of a suitable cost function

$$\begin{aligned} \Omega(\chi) = \alpha \left\{ \frac{\left\| [E^v_{tot}] - \left[E^v_{tot\,(cf)}\right] - \sum_{i=1}^{C} [G_{1,i}]\left[\tau_{D_i}\right]\left[E^v_{tot,i}\right] \right\|^2_O}{\left\| [E^v_{tot}] - \left[E^v_{inc}\right] \right\|^2_O} \right\} \\ + \beta \left\{ \frac{\left\| \left[E^v_{tot\,(cf)}\right] + [E^v_{tot}] - \sum_{i=1}^{C} [G_{1,i}]\left[\tau_{D_i}\right]\left[E^v_{tot,i}\right] \right\|^2_H}{\left\| \left[E^v_{inc}\right] \right\|^2_H} \right\} \end{aligned} \tag{7}$$

where $\alpha$ and $\beta$ are two positive regularization parameters, which allow one to weight more

the "incident" ($\beta$) or the "scattered" ($\alpha$) data depending on the uncertainties or the noise level associated with both of them. Moreover, equation (7) is the sum of two normalized least-square terms quantifying the errors when matching the scattering data.

In order to look for $\chi_{opt}$ [corresponding to the global minimum of the nonlinear cost function (7)], a suitable global minimization strategy has to be used. Towards this end, two different GA-based approaches have been developed and they will be described in the following sub-sections.

## 2.1 Hierarchical Strategy (*HS*)

Let us assume that the number of defects lying in $H$ is lower than a fixed integer $C_{max}$ ($C_{max} \geq C$). Under such a hypothesis, the hierarchical approach considers $C_{max}$ parallel reconstruction sub-processes each one aimed at investigating the presence and the characteristics of a different number of defects from 1 up to $C_{max}$. As far as the $j$-th process is concerned ($j = 1, \ldots, C_{max}$), a population of $Q_j$ trial solutions coding a fixed number of cracks, $j$, is considered

$$\underline{\chi}_j = \{\chi_{j,q};\, q = 1, \ldots, Q_j\} = \left\{ \left(j;\, \Upsilon_i,\, i = 1, ..., j;\, \left[E^v_{tot,i}\right],\, i = 1, ..., j\right)_q ;\, q = 1, \ldots, Q_j \right\}. \tag{8}$$

Starting from a set of randomly generated solutions $\underline{\chi}_j^0$, the $j$-th population iteratively evolves ($\underline{\chi}_j^{k_j} \Longrightarrow \underline{\chi}_j^{k_j+1}$, $k_j$ being the iteration index of the $j$-th process) until a stopping criterion [$k_j = K_{max}$ or $\Omega\{\chi_{j,opt}\} \leq \Omega_{th}$, $\chi_{j,min} = \arg\left\{\min_{q=1,..,Q_j}\left[\min_{k_j=1,...,K_{max}}\left(\Omega\left\{\chi_{j,q}^{k_j}\right\}\right)\right]\right\}$] is reached. At the $k_j$-th step the $(k_j+1)$-th population is generated by means of a set of suitable genetic operators denoted by $\Im\{\cdot\}$ ($\underline{\chi}_j^{k_j+1} = \Im\left\{\underline{\chi}_j^{k_j}\right\}$) and the best trial solution defined so far is stored in the array $\chi_{j,min}$. When all the $C_{max}$ processes are terminated, the convergence solution is determined as the minimum among the set of solutions $\chi_{j,min}$, $j = 1, \ldots, C$. The whole minimization procedure can be resumed by the following *pseudo-code*:

for $j = 1, ..., C_{max}$ do

$k_j = 0$

$\underline{\chi}_j^0 = \Re\left\{\underline{\chi}_j\right\}$

$\chi_{j,min} = \arg\left\{\min_{q=1,..,Q_j}\left[\Omega\left\{\chi_{j,q}^0\right\}\right]\right\}$

while $\left[(k_j < K_{max}) \text{ and } \left(\Omega\left\{\chi_{j,min}^{k_j}\right\} > \Omega_{th}\right)\right]$ do

$k_j = k_j + 1$

$\underline{\chi}_j^{k_j} = \Im\left\{\underline{\chi}_j^{k_j-1}\right\}$

$\chi_{j,min}^{k_j} = \arg\left\{\min_{q=1,..,Q_j}\left[\Omega\left\{\chi_{j,q}^{k_j}\right\}\right]\right\}$

if $\left[\Omega\left\{\chi_{j,min}^{k_j}\right\} > \Omega\left\{\chi_{j,min}^{k_j-1}\right\}\right]$ then

$\chi_{j,min} = \chi_{j,min}^{k_j-1}$

else

$\chi_{j,min} = \chi_{j,min}^{k_j}$

endif

enddo

$\chi_{opt} = \arg\left\{\min_{j=1,..,C_{max}}\left[\Omega\left\{\chi_{j,min}\right\}\right]\right\}$

enddo

where $\Re$ is the random function. As far as the implementation of the genetic operators is concerned, the hierarchical approach makes use of a *multicrack variable-length hybrid coding* (Figure 2). Each parameter of the crack in (6) is binary encoded by considering $x_i$, $y_i$, $L_i$, $W_i$, and $\theta_i$ as discrete variables: $x_i = l\Delta_B$, $l = 1, \ldots, B$; $y_i = l\Delta_B$, $l = 1, \ldots, B$; $L_i = l\Delta_D$, $l = 1, \ldots, D$; $W_i = l\Delta_D$, $l = 1, \ldots, D$, and $\theta_i = l\Delta_\Theta$, $l = 1, \ldots, \Theta$. Moreover, a real representation is used for coding the field unknowns, $E_{tot}^v(x_{p_i}, y_{p_i})$, $p_i = 1, \ldots, P_i$, $i = 1, \ldots, j$.

According to this representation, suitable stochastic operators (denoted by $\Im\{\cdot\}$) are needed. The offspring are generated from their parents by means of a customized *multicrack crossover*, whereas standard *elitism, selection* and *mutation* are adopted [19].

Because of the hybrid coding, a *single-point crossover* (*binary crossover*) $\Phi_b$ is performed with probability $\pi_b$ between the binary sequences of two parents, namely $\chi_{q_a}^{k_j}$ and $\chi_{q_b}^{k_j}$. By imposing that the cross-position "*cp*" falls only on a boundary between two adjacent genes [Figure 3($a$)], the *binary crossover* returns the following children

$$\chi_{q_a}^{k_j+1} = \{j; (\Upsilon_1)_{q_a}^{k_j}, \left[(x_i, y_i)_{q_a}^{k_j}; (L_i)_{q_a}^{k_j}; \Big|_{cp} (W_i)_{q_b}^{k_j}; (\theta_i)_{q_b}^{k_j}\right], \ldots, (\Upsilon_j)_{q_b}^{k_j}; \left[E_{tot,1}^{v}\right]_{q_a}^{k_j}, \left[E_{tot,i}^{v}\right]_{q_a}^{k_j+1}, \ldots, \left[E_{tot,j}^{v}\right]_{q_b}^{k_j}\}$$
$$\chi_{q_b}^{k_j+1} = \{j; (\Upsilon_1)_{q_b}^{k_j}, \left[(x_i, y_i)_{q_b}^{k_j}; (L_i)_{q_a}^{k_j}; \Big|_{cp} (W_i)_{q_a}^{k_j}; (\theta_i)_{q_a}^{k_j}\right], \ldots, (\Upsilon_j)_{q_a}^{k_j}; \left[E_{tot,1}^{v}\right]_{q_b}^{k_j}, \left[E_{tot,i}^{v}\right]_{q_b}^{k_j+1}, \ldots, \left[E_{tot,j}^{v}\right]_{q_a}^{k_j}\} \quad (9)$$

where $\left[E_{tot,i}^{v}\right]_{q_a}^{k_j+1}$ and $\left[E_{tot,i}^{v}\right]_{q_b}^{k_j+1}$ are computed extending to the multi-crack case the relationship reported in [20] [Eq. (11)] and pictorially described in Fig. 3($a$) ($r$ being a random number uniformly distributed in $[0; 1]$).

If the *binary crossover* $\Phi_b$ has not been applied, the *double-point crossover* is performed with probability $\pi_d$ on that part of the chromosomes concerned with the field unknowns and according to Eq. (13) of [20].

## 2.2 Integrated Strategy (*IS*)

Unlike the hierarchical approach, the integrated strategy considers a single optimization process. Towards this purpose, the population of $Q$ trial solutions is composed by "*heterogeneous*" chromosomes each of them coding a different number of cracks

$$\underline{\chi} = \{\chi_q;\, q = 1, \ldots, Q\} = \left\{C_q;\, \Upsilon_i,\, i = 1, ..., C_q;\, \left[E_{tot,i}^{v}\right],\, i = 1, ..., C_q;\, q = 1, \ldots, Q\right\} \quad (10)$$

$C_q$ being an integer value randomly chosen in the range between 1 and $C_{max}$. Moreover, starting from a randomly generated set of solutions $\underline{\chi}^0$, the iterative ($k$ being the iteration index) optimization process evolves for achieving the "*convergence*" condition ($k = K_{max}$ or $\Omega\left\{\chi_{opt}^{k}\right\} \leq \Omega_{th}$) according to the following instructions

while $\left[(k < K_{max})\ \text{and}\ \left(\Omega\left\{\chi_{opt}^{k}\right\} > \Omega_{th}\right)\right]$ do

$$k = k + 1$$
$$\underline{\chi}_b^k = \Phi_b\left[\aleph\left\{\chi_{opt}^{k-1}\right\}\right]$$
$$\underline{\chi}_o^k = \wp\left\{\chi_{opt}^{k-1}\right\}$$
$$\underline{\chi}_p^k = \left\{\underline{\chi}_b^k, \underline{\chi}_o^k, \underline{\chi}^{k-1}\right\}$$
$$\underline{\chi}^k = \Im\left\{\underline{\chi}_p^k\right\}$$
$$\chi_{opt}^k = \arg\left\{\min_{q=1,..,Q}\left[\Omega\left\{\chi_q^k\right\}\right]\right\}$$

enddo

where $\underline{\chi}_o^k$ and $\underline{\chi}_b^k$ are two populations of $\frac{Q}{2}$ trial solutions generated from the optimal trial solution reached at the $(k-1)$-th step, $\chi_{opt}^{k-1}$, by means of the operators $\wp\{\cdot\}$ and $\Phi_b[\aleph\{\cdot\}]$, respectively.

More in detail, $\underline{\chi}_b^k$ is a population whose individuals code solutions with the same number of cracks as $\chi_{opt}^{k-1}$ and it is generated by randomly modifying through the operator $\Re(\cdot)$ all genes of $\chi_{opt}^{k-1}$ except that coding $C_{opt}^{k-1}$

$$\chi_{b,q}^{k-1} = \aleph\left\{\chi_{opt}^{k-1}\right\} \triangleq \left\{C_{opt}^{k-1};\ \Re\left(\Upsilon_{opt,i}^{k-1}\right),\ i=1,...,C_{opt}^{k-1};\Re\left(\left[E_{tot,i}^{v}\right]_{opt}^{k-1}\right),\ i=1,...,C_{opt}^{k-1}\right\}_{q=1,...,\frac{Q}{2}}. \tag{11}$$

and successively, applying the *binary crossover* $\chi_{b,q}^k = \Phi_b\left\{\chi_{b,q}^{k-1}\right\}$.

As far as the sub-population $\underline{\chi}_o^k$ is concerned, it consists of $(C_{max}-1)$ equally partitioned sub-sets, each of them with individuals having the same number of cracks $C_l$, $l=1,...,(C_{max}-1)$, and different from $C_{opt}^{k-1}$. These trial solutions are generated according to the following rules:

- If an individual belongs to the $l$-th subset characterized by $C_l < C_{opt}^{k-1}$, then

$$\chi_{o,q}^k = \left\{C_l;\ \Upsilon_i^k = \Upsilon_{opt,r}^{k-1},\ i=1,...,C_l;\left[E_{tot,i}^{v}\right]^k = \left[E_{tot,s}^{v}\right]_{opt}^{k-1},\ i=1,...,C_l\right\} \tag{12}$$

  $r$ and $s$ being integer random numbers between 1 and $C_{opt}^{k-1}$ [Fig. 3($b$)];

- Otherwise (i.e., $C_l > C_{opt}^{k-1}$), the trial solution is obtained by adding suitable genes to the chromosome coding $\chi_{opt}^{k-1}$ [Fig. 3($c$)]. Randomly in that part concerned with the crack parameters and from the field distribution of the unperturbed scenario in the remaining part:

$$\chi_{o,q}^k = \left\{C_l;\ \begin{array}{ll}\Upsilon_i^k = \Upsilon_{opt,i}^{k-1}, & i=1,...,C_{opt}^{k-1}\\ \Upsilon_i^k = \Re, & i=C_{opt}^{k-1}+1,...,C_l\end{array};\ \begin{array}{ll}\left[E_{tot,i}^{v}\right]^k = \left[E_{tot,i}^{v}\right]_{opt}^{k-1}, & i=1,...,C_{opt}^{k-1}\\ \left[E_{tot,i}^{v}\right]^k = \left[E_{tot\,(cf),i}^{v}\right]_{opt}^{k-1}, & i=C_{opt}^{k-1}+1,...,C_l\end{array}\right. \tag{13}$$

Finally, each iterative loop is terminated by processing the heterogeneous population $\underline{\chi}_p^k$ through standard *selection*, *elitism*, and *mutation* (no crossover operations are performed) as described in [19][20] ($\underline{\chi}_p^k = \Im\left\{\underline{\chi}_p^{k-1}\right\}$).

# 3 Numerical Validation

As far as the validation of the proposed strategies is concerned, a numerical assessment has been carried out by considering different configurations of the defects and various characteristics of the host medium in order to verify the possibility and feasibility of dealing with more general (and probably more realistic) multiple-defects scenarios. On the other hand, the robustness against blurred scattering data has been evaluated by adding a random Gaussian noise with a fixed signal-to-noise ratio ($SNR$) to the measured field samples [20].

For quantifying the performance of the proposed implementations and because of the multiple-crack geometries, suitable error indexes have been defined extending those reported in [19]:

- *Multi-crack Localization Error*, $\delta$:

$$\delta = \frac{\sum_{c=1}^{C}}{C}\left\{\frac{\sqrt{(\widehat{x}_c - x_c)^2 + (\widehat{y}_c - y_c)^2}}{d_{max}} \times 100\right\} \tag{14}$$

  $d_{max}$ being the maximum linear dimension of $H$ and $(\widehat{x}_c, \widehat{y}_c)$ the estimated center of $c$-th crack;

- *Multi-crack Area Error*, $\Delta$:

$$\Delta = \frac{\sum_{c=1}^{C}}{C}\left\{\frac{\left|\widehat{A}_c - A_c\right|}{A_c} \times 100\right\} \tag{15}$$

Moreover, the *Precision-Recall Index*, $R$, has been evaluated for estimating the accuracy

of each strategy in detecting multiple defects and their number

$$R = \frac{\Psi_{opt}}{\Psi} \times 100 \tag{16}$$

$\Psi_{opt}$ and $\Psi$ being the number of successful detections and the total number of repeated simulations with the same geometry and conditions, respectively.

For the numerical validation, if it is not specified, the following reference scenario has been considered. A square homogeneous host medium of side $L_H = 0.8\lambda$ ($d_{max} = \sqrt{2}L_H$) characterized by a dielectric permittivity equal to $\varepsilon_H = 2.4$ and homogeneous defects ($\varepsilon_{D_i} = 1.0$ and $\sigma_{D_i} = 0.0$, $i = 1, ..., C$). Such a scenario has been illuminated by $V = 4$ directions with sources radiating electric incident fields $E^v_{inc}(x, y) = e^{-jk_0\left(x\cos\gamma^v + y\sin\gamma^v\right)}$, $\gamma^v = (v-1)\frac{2\pi}{V}$, $v = 1, ..., V$, $k_0$ being the free-space wavenumber. Furthermore, the samples of the scattered electric field have been collected at $M = 50$ equally-spaced positions located on a circle $\rho = 0.64\lambda$ in radius.

According to the guidelines suggested in [25]-[28], the following parameters for the GA-based multi-crack optimization has been assumed: $Q = 80$, $\pi_b = \pi_d = 0.7$, $\pi_m = 0.4$ (mutation probability), $K_{max} = 600$, and $\Omega_{th} = 10^{-5}$.

## 3.1 Test Case #1 - Reconstruction of a Single-Crack Configuration

As a first test case, let us consider a comparative study on the effectiveness of the multi-crack strategies versus customized single-crack techniques previously developed and carefully assessed (i.e., the $FGA$ [19] and the $IGA$ [20] approaches). Towards this purpose, an unknown defect ($C = 1$) of area $\frac{A_c}{\lambda^2}\Big\rfloor_{c=1} = 2.25 \times 10^{-2}$ has been located at $\frac{x_c}{\lambda}\Big\rfloor_{c=1} = 0.22$ and $\frac{x_c}{\lambda}\Big\rfloor_{c=1} = 0.15$ in a lossy ($\sigma_H = 0.1\,[S/m]$) host medium. Moreover, the scattering data have been blurred with an increasing level of additive noise (from $SNR = 30\,dB$ up to $SNR = 5\,dB$). Concerning multi-crack implementations, $C_{max}$ has been fixed to $C_{max} = 3$, thus the number of cracks lying in the investigation domain $H$ is an unknown, as well.

Figure 4 shows the obtained results in terms of reconstruction errors: $\delta$ [Fig. $4(a)$] and $\Delta$

[Fig. 4($b$)]. Due to the intrinsic nature both of the $GA$-based strategies and of the noise, these results are average values of the execution of each algorithm for ten independent realizations of the random process blurring the scattering data.

As expected and already demonstrated in [20], $IGA$-based approaches (i.e., the single-crack $IGA$ and the multi-crack strategies) allow a non-negligible improvement in the localization accuracy. As a matter of fact, the average value of the localization error $\langle\delta\rangle_{FGA}$ turns out to be greater than 25 %, whereas $IGA$-based algorithms provide a localization accuracy with an error index lower than 20 % whatever the noise level. Moreover, the effectiveness of $IGA$-based techniques improves ($\delta \approx 5\,\%$) for an increasing of the signal-to-noise-ratio ($SNR > 15\,dB$). Furthermore, multicrack implementations prove a better robustness against higher noisy condition ($\delta_{IGA} > \delta_{IGA-HS} \geq \delta_{IGA-IS}$ when $SNR \leq 12\,dB$) despite the enlargement of the unknowns space (since $C_{max} \neq 1$) with respect to the $IGA$ single-crack strategy.

As far as the estimation of the dimension of the defect is concerned, Fig. 4($b$) shows that the behaviors of the error figures of the single-crack $IGA$ approach and of the integrated strategy ($IG$) are quite similar in the range of noise variations, whereas the hierarchical approach ($HS$) generally does not reach the accuracy of single-crack algorithms.

## 3.2 Test Case #2 - Dependence of the Reconstruction Accuracy on the Number of Defects $C$

The second test case is aimed at evaluating the feasibility of the proposed approach in dealing with multiple-defect configurations by comparing the hierarchical and the integrated implementations. Under the assumption that $C_{max} = 3$, three geometries characterized by the presence of a number of cracks from $C = 1$ up to $C = 3$ (Fig. 5) have been considered. The position and size of each defect $D_i$, $i = 1, \ldots, C$, are summarized in Tab. I.

In order to assess the effectiveness in detecting the number of defects, the precision-recall index $R$ has been evaluated for each experiment ($C = 1, 2, 3$) and in correspondence with different signal-to-noise ratios ($SNR = 10, 20, 30\,dB$). The results of such an analysis are reported in Fig. 6. As far as the $HS$ is concerned [Fig. 6($a$)], $R\rfloor_{HS} \leq 40\,\%$

when $SNR \leq 10\,dB$ whatever the number of cracks. Otherwise ($SNR \geq 20\,dB$), the efficacy of the algorithm improves especially for a smaller value of $C$. Unlike the $HS$, the integrated implementation generally provides better performances very close to the optimal value ($R = 100\,\%$) except for "*worst*" configurations characterized by a higher noise ($SNR < 10\,dB$) and smaller defects.

The dependence of the reconstruction accuracy on the number of defects and the level of noise can be estimated from the plots shown in Fig. 7. The results are presented in terms of $\delta$ - left column [Figs. 7($a$), 7($c$), and 7($e$)] - and of $\Delta$ - right column [Figs. 7($b$), 7($d$), and 7($f$)] for $C = 1$ - first row [Figs. 7($a$) and 7($b$)], $C = 2$ - second row [Figs. 7($c$) and 7($d$)], and $C = C_{max} = 3$ - third row [Figs. 7($e$) and 7($f$)]. Both implementations provide a satisfactory localization ($\delta\rfloor_{IS} < 18\,\%$ and $\delta\rfloor_{HS} < 29\,\%$) and the centers of the cracks are accurately retrieved when $SNR > 15.0\,dB$ ($\delta < 7\,\%$).

On the other hand, the dimensioning of the defects turns out to be more difficult and the performances of the multi-crack strategies get worse. However, for comparison purposes, it should be noticed that the $IS$ considerably overcomes the $HS$ and the arising error $\Delta\rfloor_{IS}$ is always lower than 60 %. In particular, $\Delta\rfloor_{IS} < 20\,\%$ when $SNR > 15.0\,dB$.

From a computational point of view, once again, the $IS$ turns out to be more effective than the $HS$ both in terms of convergence rate and time per iteration. As one example, Figure 8 shows the plot of the required CPU-time for each iteration of a representative simulation ($C = 3$ and $SNR = 5.0\,dB$).

## 3.3 Test Case #3 - Dependence of the Reconstruction Accuracy on the Host Medium Properties ($\sigma$)

The test case #3 is devoted at evaluating the multi-crack strategies for different configurations of the host medium. Towards this end, the electric conductivity $\sigma_H$ has been varied from 0.1 $[S/m]$ up to 1.0 $[S/m]$ and the arrangement of the cracks was the same as shown in figure 5 (Tab. I).

The color-level representations of the reconstruction errors $\delta$ and $\Delta$ are reported in Figure 9. As expected, since the multi-crack strategies are based on the computation of the inhomogeneous Green's function as well as the single-crack $IGA$, both the $IS$ and the

$HS$ give accurate localizations of the defects, which result in low average values of the corresponding indexes: $\langle\delta\rangle_{HS} = 9.49\,\%$ and $\langle\delta\rangle_{IS} = 8.15\,\%$. Concerning the dependence on the conductivity of the host medium and on the $SNR$, the quality of the estimation of the defects coordinates $(x_i,\, y_i)$, $i = 1, .., C$, $C = 3$, enhances as $SNR$ increases and $\sigma$ decreases. A similar behavior holds true also for the cracks dimensioning as shown in Figs. $9(c)$-$9(d)$, but the errors significantly grow also on average ($\langle\Delta\rangle_{IS} = 52.19\,\%$ vs. $\langle\Delta\rangle_{HS} = 74.73\,\%$).

## 3.4 Test Case #4 - Dependence of the Reconstruction Accuracy on the Defects Configuration

The last test case is aimed at testing the resolution capabilities of the proposed approaches. As a matter of fact, a reliable reconstruction process should be able to distinguish adjacent defects avoiding the incorrect detection of a single crack instead of a multiple geometry. In order to verify such a feature, the same scenario as for test case #2 ($C = 3$) has been considered, but the defects have been placed closer the ones to the others as indicated in Tab. II and shown in Fig. 10.

As expected, the obtained results worsen with respect to those of Sect. 3.2. Figure $11(a)$ gives the values of the precision-recall index for different signal-to-noise ratios. The integrated approach turns out to be more efficient than the hierarchical strategy. It achieves a value of $R = 90\,\%$ in correspondence with the highest $SNR$ value and $R > 70\,\%$ whatever the noise level.

In order to point out the reliability of the $IS$ versus the $HS$, it is interesting to better detail the achieved results for a fixed $SNR$. Let us consider the case of $SNR = 10\,\%$. In such a case, the integrated approach always detects a multiple-defect configuration and the fault percentage [i.e., $F\rfloor_{IS}^{(C=2)} = 30\,\%$] is related to a geometry with two cracks. On the contrary, the probability of estimating one or two cracks is equal for the hierarchical strategy to $F\rfloor_{HS}^{(C=1)} = 13.7\,\%$ and $F\rfloor_{HS}^{(C=2)} = 46.3\,\%$ [$1 - R = \sum_{C=1}^{C_{max}} F^{(C)}$], respectively.

Concerning the reconstruction errors, by comparing the results shown in Figs. $11(b)$ and $11(c)$ to those in Figs. $7(e)$ and $7(f)$, it is evident the worsening in the localization and in the estimation of the cracks dimensions. Moreover, the capabilities in localizing and

dimensioning the defects of the $IS$ are almost independent from the noise level.

# 4 Conclusions

In this work, the problem of detecting and reconstructing multiple defects in a known host medium has been analyzed. Starting from the inverse scattering equations and by considering an effective integral formulation based on the definition of the inhomogeneous Green's function, the problem in hand has been addressed with a GA-based technique implemented through two innovative strategies.
The main features of the proposed approach are the following:

- capability to detect multiple as well as single defects;
- capability to reconstruct multiple defects different in shape as well as in dimensions;
- exploitation of the *a-priori* information and computational saving;
- capability to operate in the presence of dielectric as well as conductive host media;
- robustness to blurred data.

Concerning the methodological novelties of this work, some key-issues should be pointed out:

- specific formulation of the multi-crack reconstruction problem within the framework of inverse scattering techniques;
- original implementations of the data processing through innovative architectures based on GAs;
- definition of customized GA-operators for dealing with heterogeneous and variable-length chromosomes.

From the numerical experiments carried out on different configurations and scenarios, the following conclusions can be drawn:

- the proposed multi-crack approach proved effective providing, in its integrated implementation, both high detection accuracy, good reconstructions, and a satisfactory robustness;

- the $HS$ showed good results, but in general, they were on average inferior to those obtained with the integrated algorithm (IS). Such a behavior, although the IS chromosomes could be considered as a subset of the whole set of trial solutions coded by the HS, seems to be related to a more effective sampling of the solution space in the limited amount of iterations;

- the $IS$ revealed very good in terms of computational costs offering an acceptable trade-off between accuracy and convergence rate of the optimization process;

- the multi-crack strategies exhibited good accuracies in dealing with single-defect geometries and their performances turned out comparable with those of customized single-defect techniques;

However, although the proposed multi-crack detection technique seems to be a very promising tool for unsupervised and automatic applications, several improvements for its industrial implementation are mandatory.
Towards this end, future developments of this work will be oriented in the following directions:

- developing a procedure that parameterizes the crack by means of more general and complex descriptors;

- extending the procedure to a three-dimensional scenario;

- describing in an accurate and detailed fashion the overall measurement setup in order to take into account other sources of noise and inaccuracies in the data collection.

# Acknowledgements

A. Massa wishes to thank E. Vico for her support. Moreover, the authors are grateful to Ing. D. Pregnolato for kindly providing some numerical results of computer simulations.

# References


[1] J. L. Rose, S. P. Pelts, and X. Zhao, "Defect characterization using SH guided waves," *Review of Progress in Quantitative Nondestructive Evaluation*, D. O. Thompson and D. E. Chimenti (Eds.), vol. 20 A, pp. 142-148, 2001.

[2] C. Lehr and C. E. Liedtke, "3D reconstruction of volume defects from few X-ray images," in: *Computer analysis of images and patterns*, pp. 257-284, Springer-Verlag, Berlin, 1999.

[3] J. Hall, F. Dietrich, C. Logan, and G. Schmid, "Development of high-energy neutron imaging for use in NDE applications," *Nondestructive Characterization of Materials*, vol. IX, R. E. Green (Ed.), pp. 693-698, 1999.

[4] L. D. Favro, "Thermosonic imaging for NDE," *Review of Progress in Quantitative Nondestructive Evaluation*, D. O. Thompson and D. E. Chimenti (Eds.), vol. 20 A, pp. 478-482, 2001.

[5] S. Norton and J. Bowler, "Theory of eddy current inversion," *J. Appl. Phys.*, vol. 73, pp. 501-512, 1993.

[6] J. Ch. Bolomey and N. Joachimowicz, "Dielectric metrology via microwave tomography: present and future," *Proc. Mat. Res. Soc. Symp.*, vol. 347, pp. 259-268, 1994.

[7] J. Ch. Bolomey, "Some aspects related to the transfer of microwave sensing technology," *Proc. Mat. Res. Soc. Symp.*, vol. 430, pp. 53-58, 1996.

[8] E. Nyfors, "Industrial microwave sensors - A review," *Subsurface Sensing Technologies and Applications*, vol. 1, pp. 23-43, 2000.

[9] J. Ch. Bolomey. *Frontiers in Industrial Process Tomography*. Engineering Foundation, 1995.

[10] J. Ch. Bolomey, "Microwave imaging techniques for NDT and NDE," *Proc. Training Workshop on Advanced Microwave NDT/NDE Techniques*, Supelec/CNRS, Paris, Sept. 7-9, 1999.

[11] R. Zoughi. *Microwave Nondestructive Testing and Evaluation*, Kluwer Academic Publishers, The Netherlands, 2000.

[12] M. Tabib-Azar, "Applications of an ultra high resolution evanescent microwave imaging probe in the nondestructive testing of materials," *Materials Evaluation*, vol. 59, pp. 70-78, 2001.

[13] R. J. King and P. Stiles, "Microwave nondestructive evaluation of composites," *Review of Progress in Quantitative Nondestructive Evaluation*, vol. 3, pp.1073-81, Plenum, New York, 1984.

[14] S. J. Lockwood and H. Lee, "Pulse-echo microwave imaging for NDE of civil structures: Image reconstruction, enhancement, and object recognition," *Int. J. Imaging Systems Technol.*, vol. 8, pp. 407-412, 1997.

[15] K. Meyer, K. J. Langenberg, and R. Schneider, "Microwave imaging of defects in solids," *Proc. 21st Annual Review of Progress in Quantitative NDE*, Snowmass Village, Colorado, USA, July 31 - Aug. 5, 1994.

[16] W. C. Chew and Y. M. Wang, "Reconstruction of two-dimensional permittivity distribution using the distorted Born iterative method," *IEEE Trans. on Medical Imaging*, vol. 9, pp. 218-225, 1990.

[17] C. C. Chiu and P. T. Liu, "Image reconstruction of a perfectly conducting cylinder by the genetic algorithm," *IEE Proc. Microw. Antennas Propag.*, vol. 3, p. 143, 1996.

[18] K. Belkebir, Ch. Pichot, J. Ch. Bolomey, P. Berthaud, G. Gottard, X. Derobert and G. Fauchoux, "Microwave tomography system for reinforced concrete structures," *Proc. 24th European Microwave Conf.*, Cannes, France, pp. 1209-1214, 1994.

[19] S. Caorsi, A. Massa, and M. Pastorino, "A crack identification microwave procedure based on a genetic algorithm for nondestructive testing," *IEEE Trans. Antennas Propagat.*, vol. 49, pp. 1812-1820, 2001.

[20] S. Caorsi, A. Massa, M. Pastorino, and M. Donelli, "Improved microwave imaging procedure for nondestructive evaluations of two-dimensional structures," *IEEE Trans. Antennas Propagat.*, vol. 52, pp. 1386-1397, 2004.

[21] M. Benedetti, M. Donelli, G. Franceschini, M. Pastorino, and A. Massa, "Effective exploitation of the a-priori information through a microwave imaging procedure based on the SMW for NDE/NDT applications," *IEEE Trans. Geosci. Remote Sensing*, vol. 43, pp. 2584-2592, 2005.

[22] A. Ishimaru, *Electromagnetic Wave, Propagation, Radiation and Scattering*. Englewood Cliffs, NJ: Prentice-Hall, 1991.

[23] S. Caorsi, G. L. Gragnani, M. Pastorino, and M. Rebagliati, "A model-driven approach to microwave diagnostics in biomedical applications," *IEEE Trans. Microwave Theory Tech.*, vol. 44, pp. 1910-1920, 1996.

[24] J. H. Richmond, "Scattering by a dielectric cylinder of arbitrary cross-section shape," *IEEE Trans. Antennas Propagat.*, vol. 13, pp. 334-341, 1965.

[25] R. L. Haupt and S. E. Haupt. *Practical Genetic Algorithms*, John Wiley & Sons Inc., New York, 1998.

[26] D. S. Weile and E. Michielssen, "Genetic algorithm optimization applied to electromagnetics: a review," *IEEE Trans. Antennas Propagat.*, vol. 45, pp. 343-353, 1997.

[27] J. M. Johnson and Y. Rahmat-Samii, "Genetic algorithms in engineering electromagnetics," *IEEE Trans. Antennas Propagat. Magaz.*, vol. 39, pp. 7-25, 1997.

[28] Y. Rahmat-Samii and E. Michielssen. *Electromagnetic Optimization by Genetic Algorithms*, John Wiley & Sons Inc., New York, 1999.

# FIGURE CAPTIONS

- **Figure 1.** Multi-crack problem geometry ($C = 2$).
- **Figure 2.** Example of a *multicrack hybrid coded variable-length* chromosome.
- **Figure 3.** Example of $(a)$ the *binary crossover.* Generation of trial solutions of the sub-population $\underline{\chi}_o^k$ when $(b)$ $C_l < C_{opt}^{k-1}$ and when $(c)$ $C_l > C_{opt}^{k-1}$.
- **Figure 4.** Test Case #1. Behavior of $(a)$ $\delta$ and $(b)$ $\Delta$ versus $SNR$ when $C = 1$ and for $FGA$, $IGA$, $HS$, and $IS$.
- **Figure 5.** Test Case #2. Reference geometry.
- **Figure 6.** Test Case #2. Behavior of the *precision-recall index* $R$: $(a)$ Hierarchical Strategy and $(b)$ and Integrated Strategy.
- **Figure 7.** Test Case #2. Behavior of reconstruction errors versus $SNR$ for different number of defects. $C = 1$: $(a)$ $\delta$ and $(b)$ $\Delta$; $C = 2$: $(c)$ $\delta$ and $(d)$ $\Delta$; $C = 3$: $(e)$ $\delta$ and $(f)$ $\Delta$.
- **Figure 8.** CPU times. Comparison among the $IS$ and the $HS$ when $C = 3$ and $SNR = 5\,dB$.
- **Figure 9.** Test Case #3. Behavior of the reconstruction errors versus $SNR$ and the conductivity of the host medium, $\sigma_H$. *Hierarchical Strategy*: $(a)$ localization error $\delta$ and $(b)$ area error $\Delta$. *Integrated Strategy*: $(c)$ localization error $\delta$ and $(d)$ area error $\Delta$.
- **Figure 10.** Test Case #4. Reference geometry.
- **Figure 11.** Test Case #4. Behavior of the error indexes versus $SNR$ for the $HS$ and the $IS$: $(a)$ precision-recall index $R$ , $(b)$ localization error $\delta$, and $(c)$ area error $\Delta$.

# TABLE CAPTIONS

- **Table I.** Test Cases #1 and #2 - Positions and sizes of the defects.
- **Table II.** Test Case #3 - Positions and sizes of the defects.

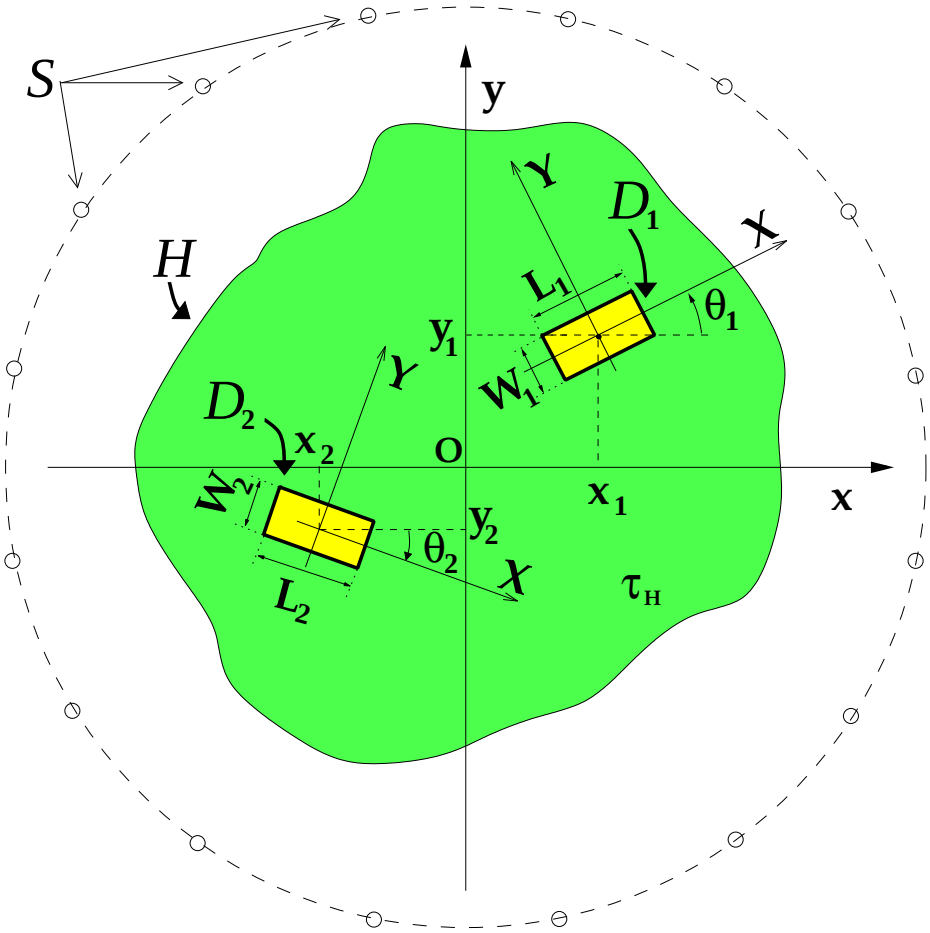


**Fig. 1 - M. Benedetti *et al.***, "Multicrack Detection in Two-Dimensional ..."

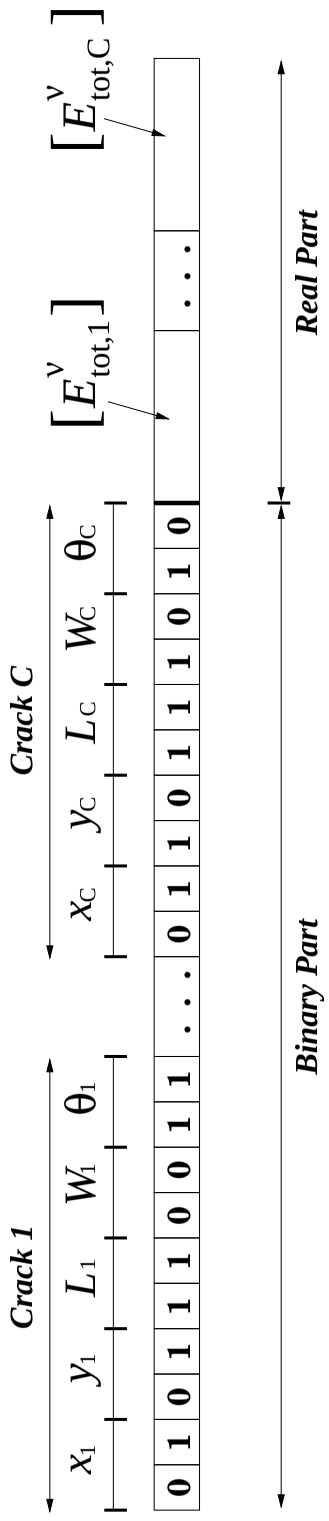


**Fig. 2 - M. Benedetti *et al.***, "Multicrack Detection in Two-Dimensional ..."

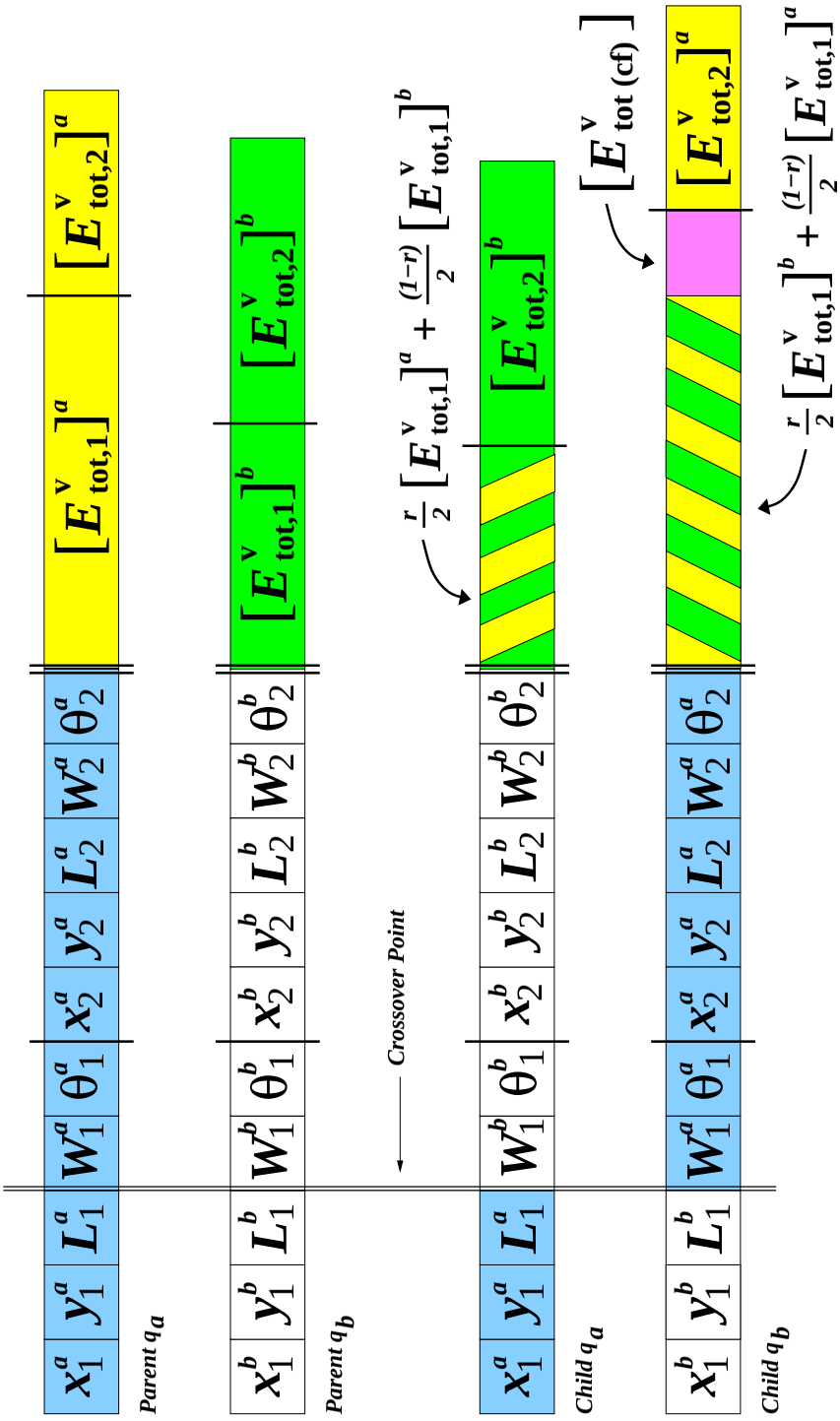


**Fig. 3 (*I*)** - **M. Benedetti *et al.***, "Multicrack Detection in Two-Dimensional ..."

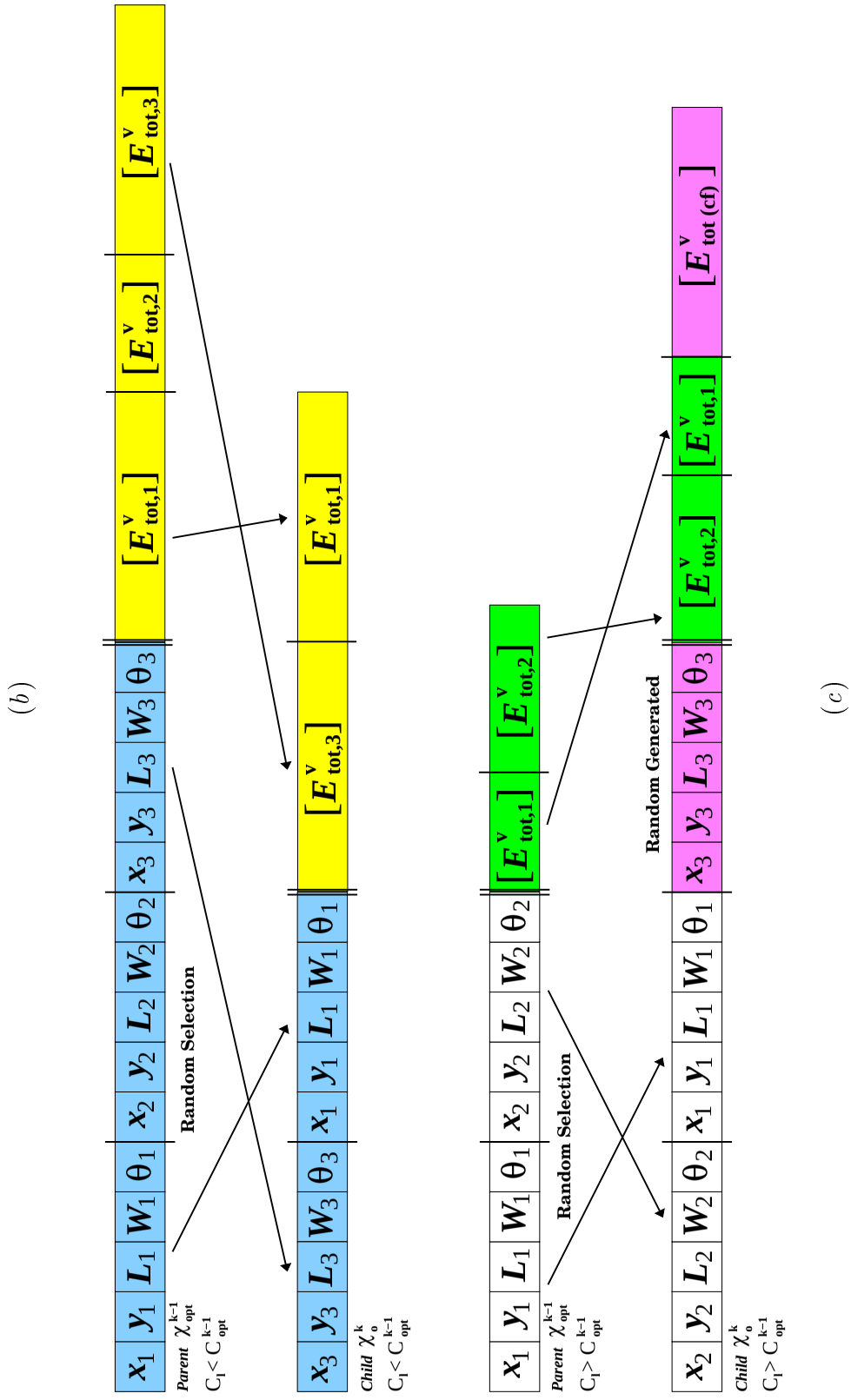


**Fig. 3 (*II*)** - **M. Benedetti *et al.***, "Multicrack Detection in Two-Dimensional ..."

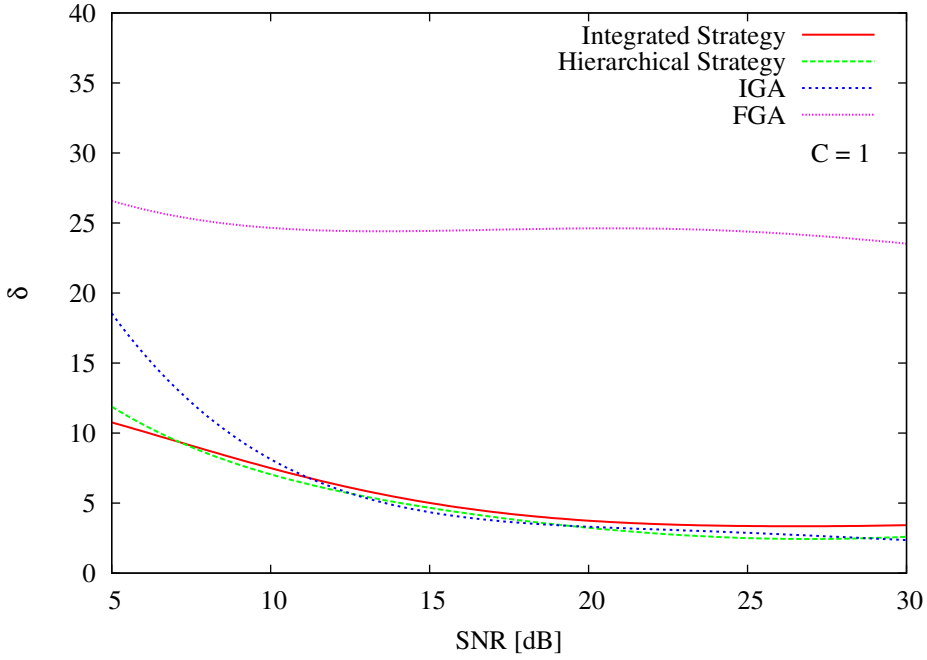


$(a)$

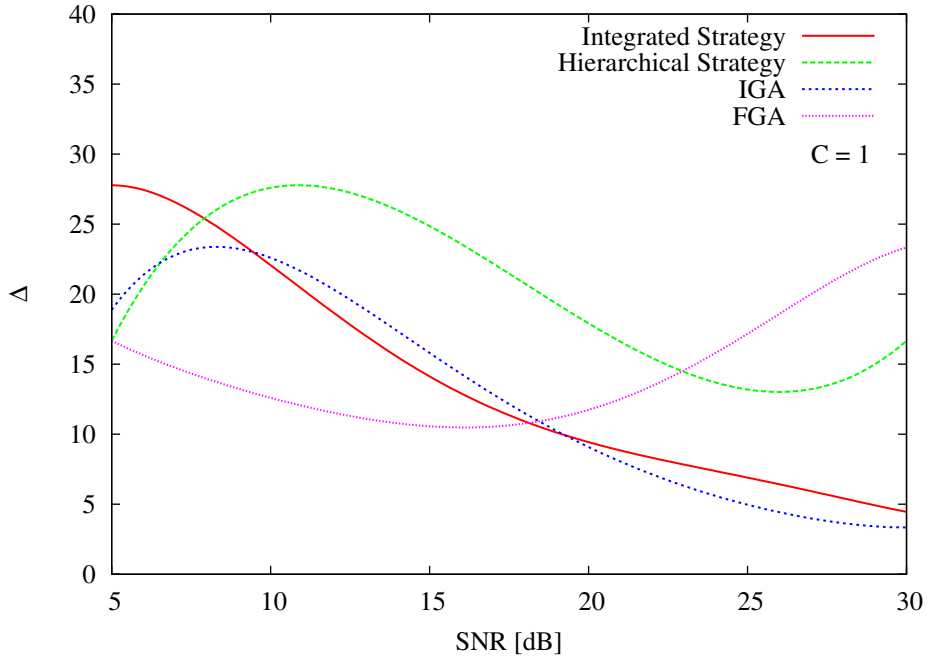


$(b)$

**Fig. 4 - M. Benedetti *et al.***, "Multicrack Detection in Two-Dimensional ..."

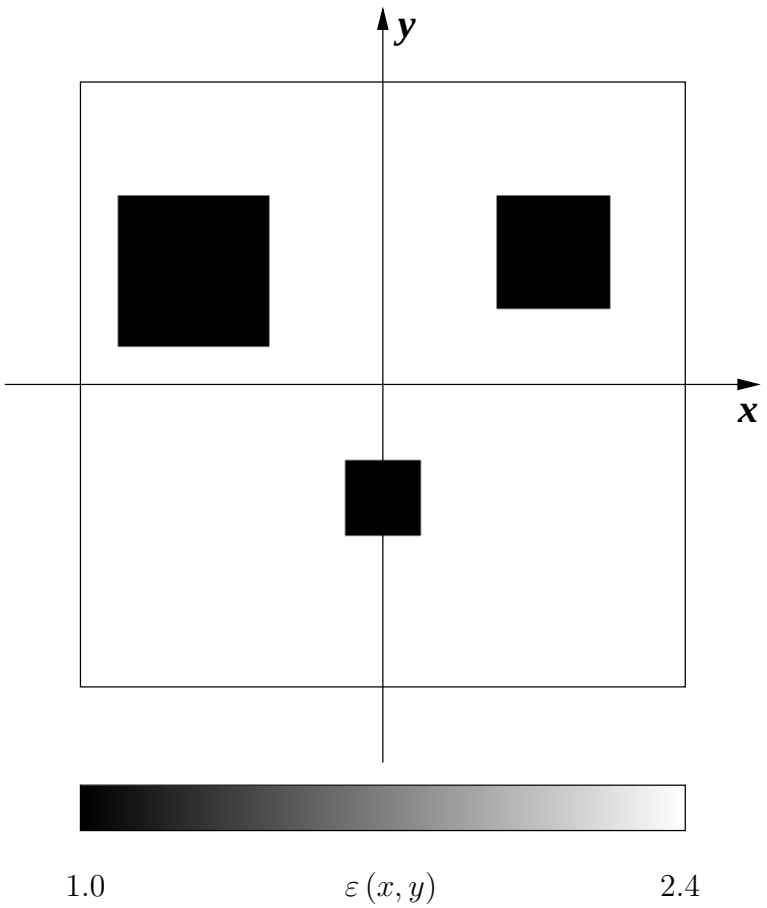


**Fig. 5 - M. Benedetti *et al.***, "Multicrack Detection in Two-Dimensional ..."

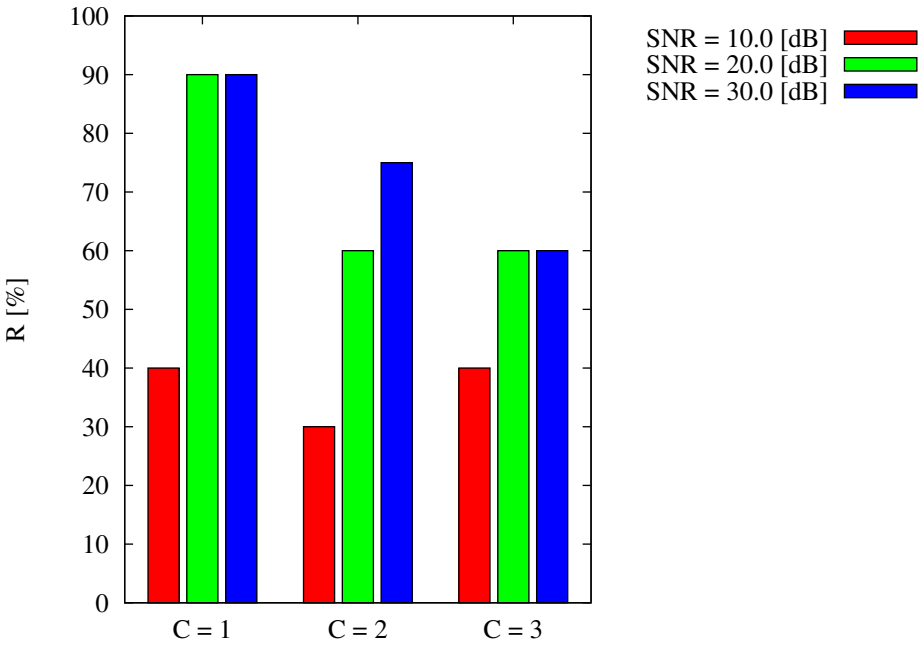


$(a)$

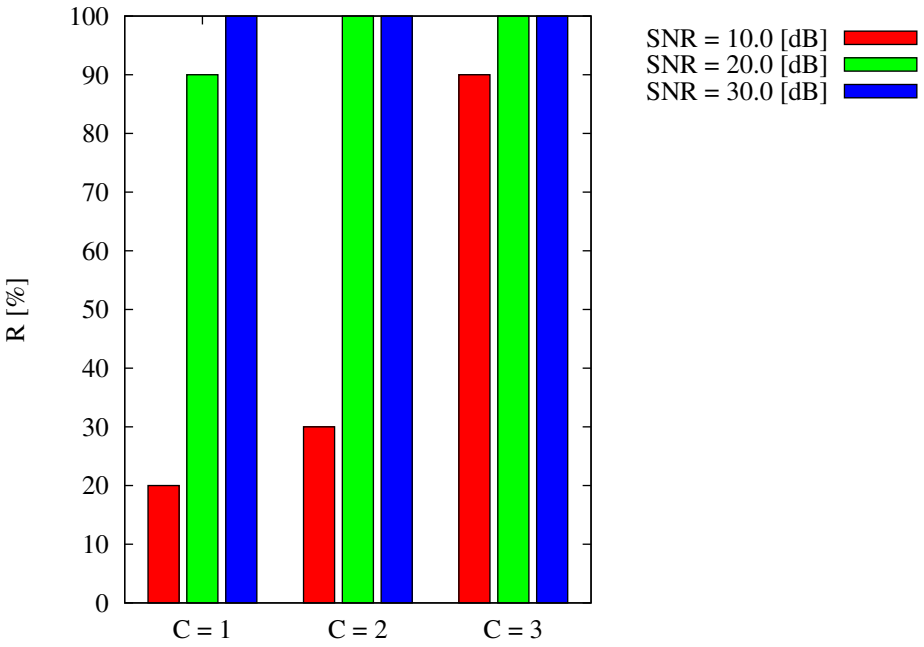


$(b)$

**Fig. 6 - M. Benedetti *et al.***, "Multicrack Detection in Two-Dimensional ..."

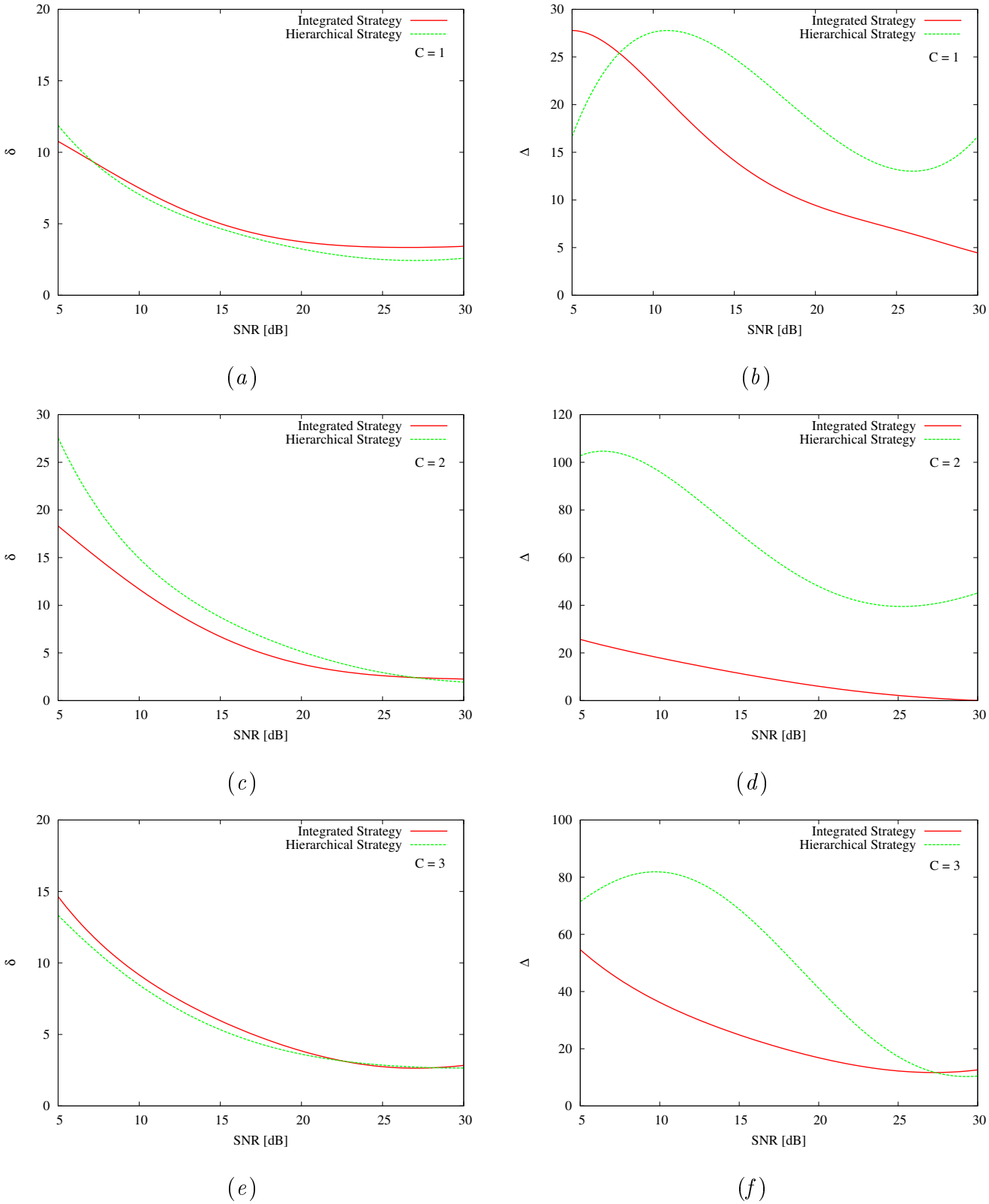


**Fig. 7 - M. Benedetti *et al.***, "Multicrack Detection in Two-Dimensional ..."

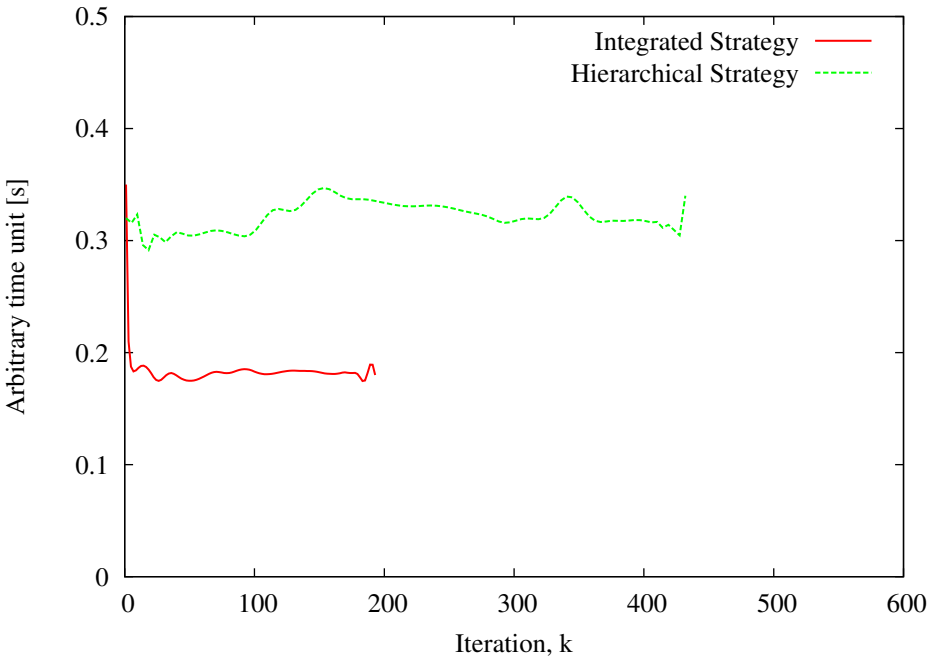


**Fig. 8 - M. Benedetti *et al.***, "Multicrack Detection in Two-Dimensional ..."

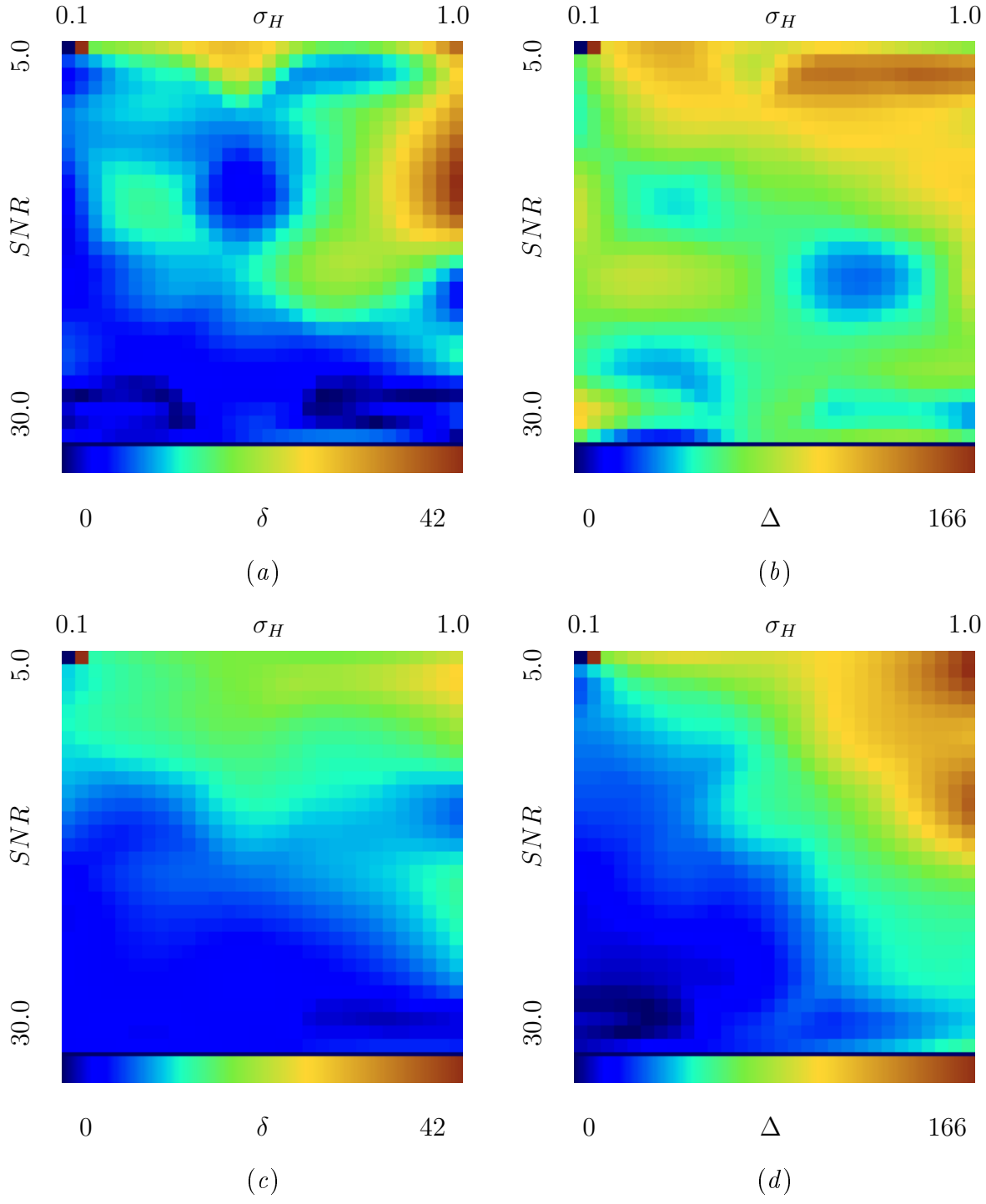


**Fig. 9 - M. Benedetti *et al.***, "Multicrack Detection in Two-Dimensional ..."

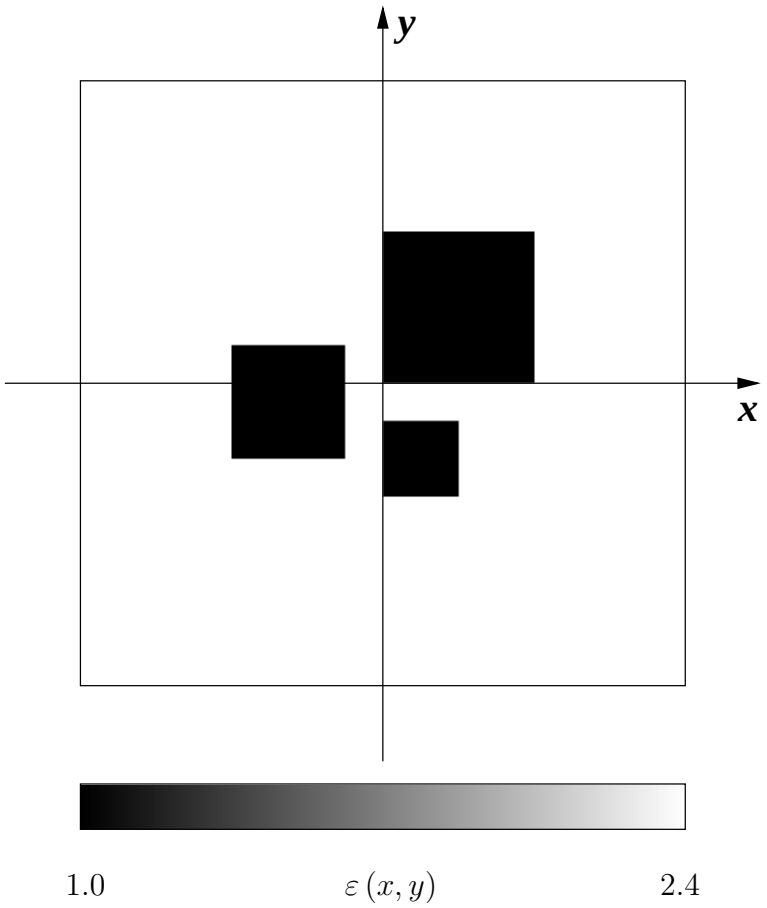


**Fig. 10 - M. Benedetti *et al.***, "Multicrack Detection in Two-Dimensional ..."

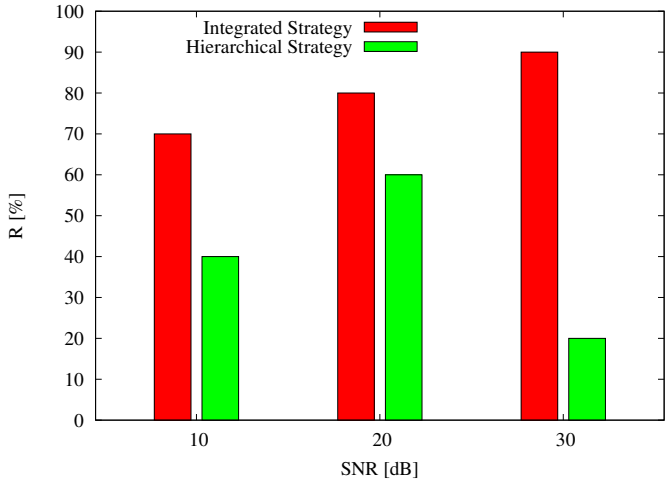


$(a)$

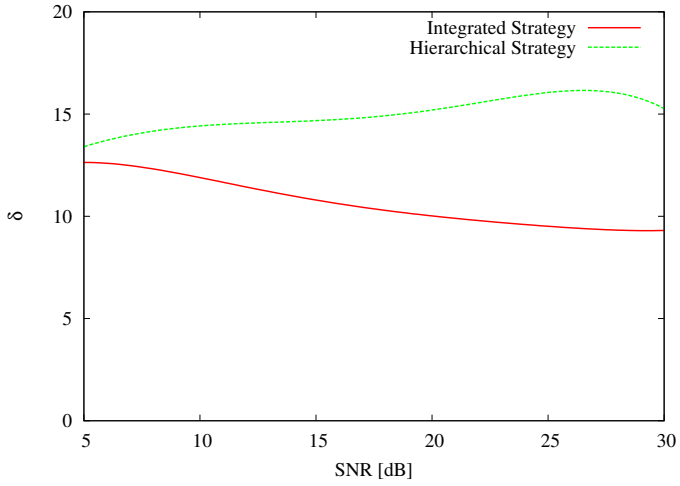


$(b)$

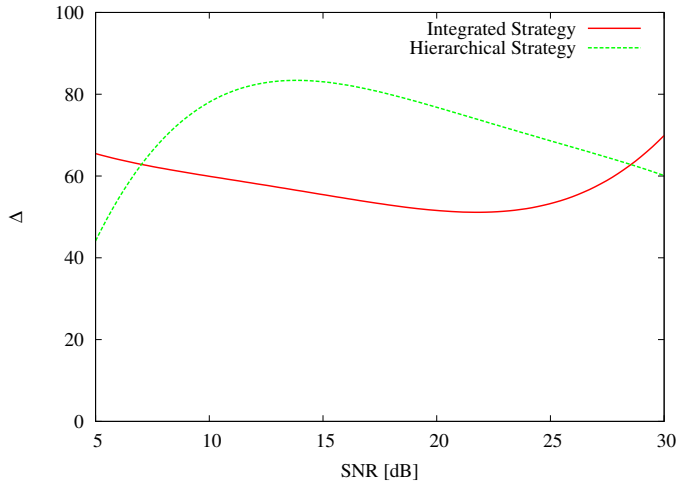


$(c)$

**Fig. 11 - M. Benedetti *et al.***, "Multicrack Detection in Two-Dimensional ..."

| | $\frac{x_c}{\lambda}$ | $\frac{y_c}{\lambda}$ | $\frac{A_c}{\lambda^2}$ |
|---|---|---|---|
| $c = 1$ | $0.22$ | $0.15$ | $0.0225$ |
| $c = 2$ | $0.0$ | $-0.15$ | $0.01$ |
| $c = 3$ | $-0.26$ | $0.15$ | $0.04$ |

**Tab. I - M. Benedetti *et al.***, "Multicrack Detection in Two-Dimensional ..."

| | $\frac{x_c}{\lambda}$ | $\frac{y_c}{\lambda}$ | $\frac{A_c}{\lambda^2}$ |
|---|---|---|---|
| $c = 1$ | $0.102$ | $0.102$ | $0.04$ |
| $c = 2$ | $0.046$ | $-0.102$ | $0.01$ |
| $c = 3$ | $-0.102$ | $0.046$ | $0.0225$ |

**Tab. II - M. Benedetti *et al.***, "Multicrack Detection in Two-Dimensional ..."